Title

Photoionization Efficiencies of Five Polycyclic Aromatic Hydrocarbons

Journal

The Journal of Physical Chemistry A, 121(23)

ISSN

1089-5639

Authors

Johansson, K Olof

Campbell, Matthew F

Elvati, Paolo

et al.

Publication Date

2017-06-15

DOI

10.1021/acs.jpca.7b02991

Peer reviewed

Photoionization Efficiencies of Five Polycyclic Aromatic Hydrocarbons

K. Olof Johansson,[1] Matthew F. Campbell,[1] Paolo Elvati,[2] Paul E. Schrader,[1] Judit Zádor,[1] Nicole K. Richards-Henderson,[3] Kevin R. Wilson,[3] Angela Violi,[2,4] and Hope A. Michelsen*[1]*

[1]Combustion Research Facility, Sandia National Laboratories, Livermore, CA 94550, USA.

[2]Department of Mechanical Engineering, University of Michigan, Ann Arbor, MI 48109, USA.

[3]Chemical Sciences Division, Lawrence Berkeley National Laboratory, Berkeley, CA 94720, USA.

[4]Departments of Chemical Engineering, Macromolecular Science and Engineering, Biophysics Program, University of Michigan, Ann Arbor, MI 48109, USA.

AUTHOR INFORMATION

Corresponding Author

*Correspondence and requests for materials should be addressed to H.A.M. (hamiche@sandia.gov) or K.O.J. (okjohan@sandia.gov).

ABSTRACT

We have measured photoionization-efficiency curves for pyrene, fluoranthene, chrysene, perylene, and coronene in the photon-energy range 7.5-10.2 eV and derived their photoionization cross-section curves in this energy range. All measurements were performed using tunable vacuum ultraviolet (VUV) radiation generated at the Advanced Light Source synchrotron at Lawrence Berkeley National Laboratory. The VUV radiation was used for photoionization and detection was performed using a time-of-flight mass spectrometer. We measured the photoionization efficiency of 2,5-dimethylfuran simultaneously with those of pyrene, fluoranthene, chrysene, perylene, and coronene to obtain references of the photon flux during each measurement from the known photoionization cross-section curve of 2,5-dimethylfuran.

INTRODUCTION

Polycyclic aromatic hydrocarbon (PAH) chemistry is important in many fields. On Earth, PAHs are predominantly produced during the incomplete combustion of hydrocarbon fuels.[1-2] When released into the atmosphere, they play a significant role in degradation of air quality.[2-3] They tend to be toxic and carcinogenic and thus pose a risk to human health.[1-3] In addition, PAHs are important precursors to soot formation.[4-7]

PAHs are also hypothesized to be abundant in interstellar media.[8-12] The low ionization energies of these species make them susceptible to the photoelectric effect upon absorption of a photon in the far-ultraviolet.[13-14] In addition, their planar structures allow photoelectrons to readily escape and contribute to the observed heating of interstellar gas,[13, 15] which is also contributed to by PAH clusters and small graphitic grains.[16] Thus, early studies on single-photon photoionization of the PAHs pyrene and coronene were conducted over a broad photon-energy range and aimed at facilitating estimations of interstellar-gas heating as a result of photoionization.[17]

Some PAH investigations are of relevance to more than one research community. Recently, the formation mechanisms of the two-ring species naphthalene and indene were studied over temperature and pressure ranges that span the extreme environments relevant to many flames and interstellar media.[18] It was found that the reactions are critically dependent on temperature and pressure, and the reaction channels may therefore differ between flames, cold molecular clouds, and hot interstellar environments.[18] Indene formation has also been studied experimentally in a high-temperature reactor by reacting phenyl radicals with propyne and allene.[19] The reaction products were measured using time-of-flight mass spectrometry coupled with near-threshold vacuum-ultraviolet (VUV) single-photon photoionization. Indene was separated from its isomers

among the reaction products by analyzing the photoionization-efficiency (PIE) curves recorded by tuning the photon energy.[19] In a similar fashion, naphthalene formation was studied by reacting phenyl radicals with acetylene using near-threshold VUV photoionization time-of-flight mass spectrometry, and PIE curves were used to verify the formation of naphthalene.[20] The curve shape measured during PIE studies is determined by the photoionization cross-section curves of signal-contributing isomers modified by the photon flux of the photon source at different photon energies.

Despite numerous studies on PAH ionization energies, absorption cross sections, photoionization quantum yields, relative and absolute photoionization cross sections, and photodissociation rates, only a limited number of PAHs have had their photoionization cross sections measured, calculated, or estimated over wide photon-energy ranges. The absorption-cross section curves, however, have been calculated for many neutrals and their cations and dications.[21-22] Nonetheless, the photoionization cross sections are not directly accessible from the absorption cross sections because the photoionization yields are less than unity for photon energies below ~17 eV.[17, 23] Instead, photoionization cross sections can be estimated using semi-empirical approaches, for example, by combining calculated VUV absorption cross sections of neutral PAHs with the photoionization-yield estimation equation provided by Jochims *et al.*,[23] or by using the atom-pair additivity model of Bobeldijk *et al.*[24] For many purposes estimations may suffice; many PAHs are structurally similar, which generally leads to similar photoionization properties, and even simple estimations can be accurate in obtaining photoionization cross sections that are representative for these species.

Detailed information on the photoionization cross-section curve shapes of individual PAHs can sometimes provide chemical insight even when large numbers of isomers with ionization energies and photoionization curve shapes that are not easily distinguishable preclude reliable isomer

assignments from PIE analysis. For example, the pyrene photoionization cross-section curve measured by Verstraete *et al.*[17] was recently used to prove that $C_{16}H_{10}$ isomers other than pyrene were detected using mass spectrometry on soot-precursor species extracted from ethylene flames.[25] A similar result was obtained in an acetylene counter-flow diffusion flame by comparing an estimated pyrene photoionization cross-section curve[26] to the measured PIE curve from soot samples.[27] These results show that the use of tunable VUV radiation for near-threshold single-photon photoionization can provide important, albeit somewhat limited, chemical compositional information if precise photoionization cross-section curve shapes are known.

The present paper presents PIE measurements of pyrene, fluoranthene, chrysene, perylene, and coronene between 7.5 and 10.2 eV. We derived the photoionization cross-section curves for these PAHs by estimating the ratio between the photoionization cross sections at ~10 and 17 eV. At 17 eV, the photoionization cross section is ~25 Mb per carbon atom. Our photoionization cross-section curves for pyrene and coronene demonstrate good agreement with photoionization cross-section curves measured previously.[17,28]

EXPERIMENTAL SECTION

Measurements were performed at the Chemical Dynamics Beamline at the Advanced Light Source at Lawrence Berkeley National Laboratory in Berkeley, CA, USA. We used a time-of-flight aerosol mass spectrometer. It consists of three pumping stages, and the sample is injected *via* an aerodynamic lens system (ADL).[29-31] The pressure behind the inlet nozzle feeding the ADL is about 1 to 2 Torr. The outlet of the ADL is in the first stage vacuum chamber (4.5-inch spherical cube from Kimball Physics). The ADL acts as a filter against gas-phase molecules and small

particles; it focuses particles larger than ~50 nm into a beam while small particles and gas-phase molecules follow Brownian motion and are pumped out by the turbo-molecular vacuum pumps.[30-31]

The second vacuum chamber (4.5-inch spherical cube from Kimball Physics) acts as a differential pumping stage. The third chamber is the ionization chamber (custom 10-inch diameter cylindrical vessel with multiple conflat ports), and it has an operating pressure of ~7×10^{-7} Torr. The particles focused by the ADL impinge on a copper target that is heated to ~300 ˚C and located near the center of the ionization chamber. After striking the target, species that are weakly bound to the particles are vaporized. A quasi-continuous beam of tunable VUV radiation from the synchrotron passes ~1.9 mm in front of the aerosol target and is used for single-photon ionization of vaporized species. The resulting ions are pulse extracted into the time-of-flight drift tube at a rate of 15 kHz.

A 30-torr Ar gas filter and a magnesium fluoride (MgF_2) window were used in the beam path to prevent high harmonics of the synchrotron radiation from entering the ionization region of the mass spectrometer. The MgF_2 window prevented measurements significantly beyond ~10.2 eV because of its VUV absorption characteristics. The photon-energy distribution was relatively broad (~0.2 eV full-width at half-maximum). In addition, the photon-energy distribution was sitting on top of a broad photon-energy plateau of lower photon flux. Furthermore, there was a significant amount of visible light superimposed on the VUV radiation.

PAH Measurements

We performed photoionization cross-section measurements on pyrene, fluoranthene, chrysene, perylene, and coronene in the photon-energy range 7.5-10.2 eV. A photon-flux reference was necessary because the flux is different at different photon energies. The visible light superimposed on the VUV radiation was significant enough to preclude use of a photodiode to directly measure the VUV-photon flux inside the ionization chamber. Instead we used the signal from a constant flow of 2,5-dimethylfuran as the reference. The ion signal from the 2,5-dimethylfuran flow was directly related to the VUV-photon flux, because only VUV photons contributed to the ionization process. The selection of 2,5-dimethylfuran as the reference substance was based on the following criteria: (1) the reference substance should not be in a condensed phase at room temperature under vacuum in order to avoid condensation, (2) its room-temperature vapor pressure should be high enough to yield sufficient signal, (3) its photoionization cross-section curve should be known and available in the literature (we used the data published by Xie *et al*.[32]), (4) it should ionize at photon energies below 8 eV (2,5-dimethylfuran ionizes at energies ≥7.8 eV[32]), and (5) its molecular mass should be different from any of the PAHs under study (Table 1 summarizes some information about the five PAHs and 2,5-dimethylfuran). In order to generate a constant flow of 2,5-dimethylfuran, ~50 ml of its liquid was contained in an air-evacuated stainless-steel vessel. This vessel was connected to the calibration port of the mass spectrometer *via* a precision leak valve. Gas-phase 2,5-dimethylfuran that evaporated from the liquid was transported directly to the ionization region of the mass spectrometer through a small-gauge tube. The gas flow was driven by the pressure difference between the vessel containing 2,5-dimethylfuran and the ionization region of the mass spectrometer. The reference gas was injected simultaneously with the PAH species introduced through the ADL, and both signals were recorded concurrently. The reason for

not introducing the PAHs through the same port as the 2,5-dimethylfuran was to avoid condensation of the PAHs in the small-gauge tube that constituted the calibration line.

Table 1. PAH samples and the 2,5-dimethylfuran reference

Species	Condensed molecular formula	Molecular weight (u)*	Supplier article/product	Purity stated by supplier	Melting point/range (˚C)†
Pyrene	$C_{16}H_{10}$	202.07825	Sigma-Aldrich 185515	98% (FTNMR)	145-148
Fluoranthene	$C_{16}H_{10}$	202.07825	Sigma-Aldrich 11474	99.5% (mass)	105-110
Chrysene	$C_{18}H_{12}$	228.09390	Sigma-Aldrich 35754	99.9% (area, GC)	252-254
Perylene	$C_{20}H_{12}$	252.09390	Sigma-Aldrich 45798	99.9% (area, HPLC)	276-279
Coronene	$C_{24}H_{12}$	300.09390	Sigma-Aldrich 335355	99% (FT-NMR)	428
2,5-dimethylfuran	C_6H_8O	96.057515	Sigma-Aldrich 177717	98.5% (area GC)	-62

*Stated masses are for species containing only the most abundant carbon and hydrogen isotopes, *i.e.*, ^{12}C (12.000000 u)[33] and ^{1}H (1.007825 u)[33].

†Information taken from supplier's webpage.

All the PIE curves for a single PAH species were recorded in rapid succession over a time span of ~80-200 min. We compared the PIE-curve shapes for 2,5-dimethylfuran recorded simultaneously with the PIE curves for each PAH. We observed no change in 2,5-dimethylfuran PIE-curve shape over this measurement-time period, and thus averaged the same number of measurements of the 2,5-dimethylfuran signal curve as was used for the PAH species. We convolved the 2,5-dimethylfuran photoionization cross-section curve measured by Xie *et al*.[32] with our photon-energy distribution function at 9.2 eV. A convolution is not entirely correct, because the photon-energy distribution is expected to change slightly when the photon energy is tuned, partly because the transmission function of the MgF_2 window changes with the photon energy. The error introduced by this effect should be small and was neglected. The photoionization cross-section curve obtained after convolution with the photon-energy distribution is hereafter referred to as the reference 2,5-dimethylfuran curve.

Following convolution, the averaged 2,5-dimethylfuran PIE curves were fit to the reference 2,5-dimethylfuran curve between 7.5 and 9.0 eV. Three (energy-independent) parameters were used in the fit; a scaling factor, an offset, and an energy shift. The energy shift was included in order to account for small mismatches in the exact photon energy between our measurements and the measurement performed by Xie *et al*.[32] The energy shifts obtained from the fits were always between 0.006 and 0.016 eV, *i.e.*, more than 10 times smaller than the full-width at half maximum of the present photon-energy distribution. The averaged 2,5-dimethylfuran PIE curves were corrected for the energy shifts, scaled by the scaling factors from the fits, and background corrected. Photon-flux reference curves were then derived as the functions that overlaid the reference 2,5-dimethylfuran curve onto the corrected 2,5-dimethylfuran PIE curves. A typical example of a photon-flux reference curve is shown in Fig. 1. The error bars are 95% confidence

intervals of the standard errors of the mean under the assumption of normally distributed sample distributions. The upper and lower confidence-interval limits were calculated as $\bar{x} \pm 1.96\sigma/\sqrt{n}$, where $\bar{x}$ is the mean value, σ is the standard deviation, and n is the number of sampled curves. Potential errors in the shape of the photoionization cross-section curve of 2,5-dimethylfuran, taken from the work of Xie *et al*.,[32] are not known to us and therefore could not be included in the error analysis. The ionization threshold of 2,5-dimethylfuran is 7.8 eV.[32] Therefore, the values derived for the photon-flux reference at and below 7.8 eV were considered unreliable, despite the fact that some 2,5-dimethylfuran signal was measured below 7.8 eV because of the broad photon-energy distribution. Hence, the first four points of Fig. 1, *i.e.*, the values at 7.5, 7.6, 7.7, and 7.8 eV have been set to 1.

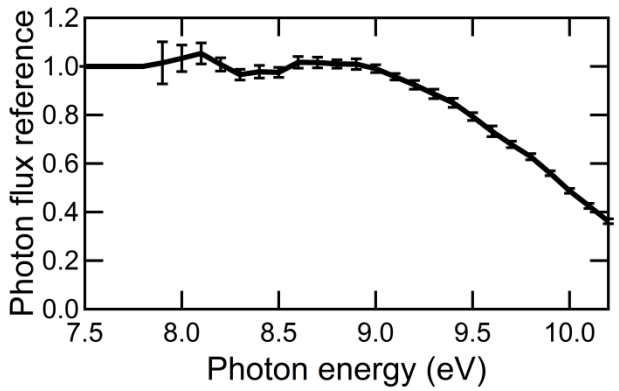

Fig. 1. A typical photon-flux reference curve showing the relative photon flux as a function of the photon energy.

The five PAHs studied are all in the solid phase under ambient conditions. They were kept in separate U-shaped borosilicate glass tubes, and one species was measured at a time. The U-shaped tubes are ~15 cm tall and ~7.5 cm wide and have outer diameters (OD) of 12.7 mm and inner diameters (ID) of 9.5 mm. They were wrapped with heat bands and heated to ~60-150 ˚C; the operating temperature was dictated by the volatility of the PAH under study. Figure 2 shows a

schematic diagram of the experimental setup. A constant flow of NaCl particles in dry N_2 passed through the U-shaped tube containing the PAH solid and vapor. The NaCl particles acted as condensation nuclei for the PAH molecules in order to efficiently transport PAHs to the ionization region of the mass spectrometer. The NaCl-N_2 flow was generated using an atomizer followed by two diffusion dryers. The atomization liquid was a solution of 0.5% (by mass) NaCl in de-ionized water, and the atomization flow was ~3 standard liters/minute (slm) N_2 (gas-flow rates referenced to 0 ˚C and 101325 Pa). Only a fraction of the 3-slm N_2-atomization flow was directed through the sampling line, *i.e.*, through the U-shaped PAH-containing tube, and into the ADL. We used a Venturi nozzle to remove the portion of the NaCl-N_2 flow that did not go to the sampling line and a proportional-integral-derivative (PID) regulator to adjust the N_2-flow rate through the Venturi pump to control the pumping speed of the nozzle. The flow rate into the sampling line was controlled by the pumping speed of the Venturi pump, which could be adjusted without changing the concentration of the NaCl-N_2 gas going into the sampling line.

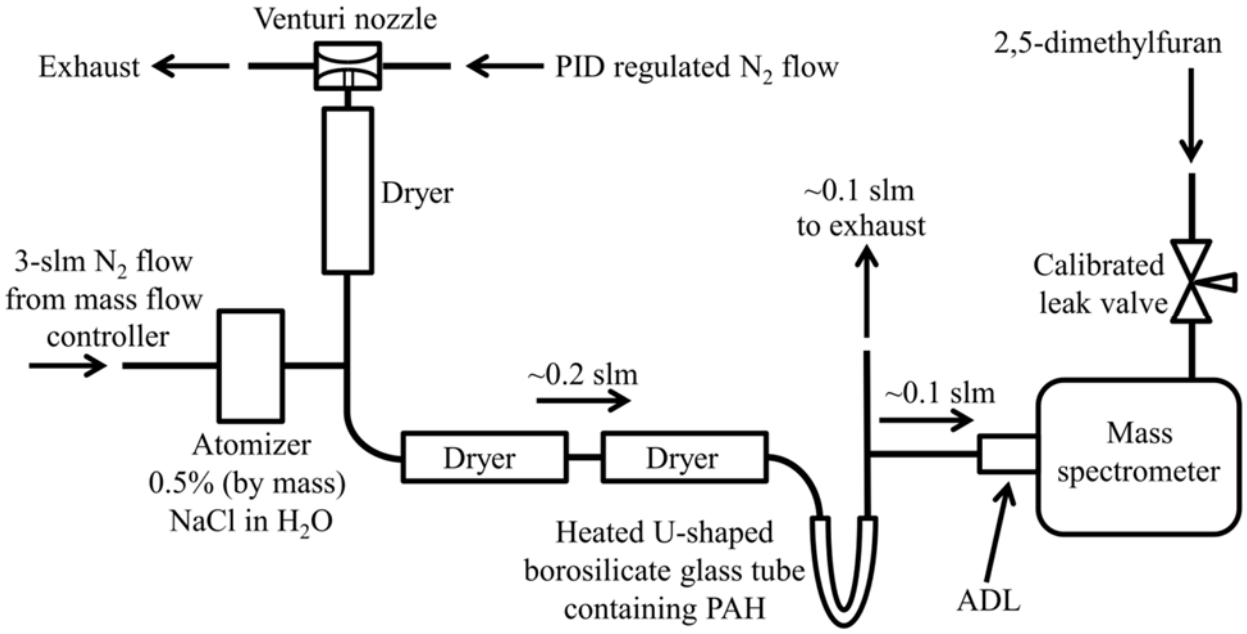

Fig. 2. Schematic diagram of the experimental setup. Flow rates are given in standard liters/min (slm) referenced to 0 ˚C and 101325 Pa.

We tested naphthalene in addition to the five PAHs listed above, but the high volatility of naphthalene prevented it from remaining condensed on the NaCl particles all the way to the aerosol target, and the naphthalene signal was too low to measure.

RESULTS AND DISCUSSION

The averages of the raw PIE scans recorded for pyrene ($C_{16}H_{10}$), fluoranthene ($C_{16}H_{10}$), chrysene ($C_{18}H_{12}$), perylene ($C_{20}H_{12}$), and coronene ($C_{24}H_{12}$) are shown in Fig. 3a-e. These curves represent averages of 13 (pyrene), 12 (fluoranthene), 8 (chrysene), 11 (perylene), and 19 (coronene) measurements and have not been corrected for differences in the photon flux at different photon energies. The strong signal decline at photon energies larger than ~9.8 eV, which yields a maximum somewhere between 9.6 and 9.8 eV for all the curves in Fig. 3a-e, is largely due to absorption in the MgF_2 window and goes away when the curves are corrected for the drop in photon flux at high photon energies. The error bars are 95% confidence intervals of the standard errors of the mean. The precision of the measurements is high, as demonstrated by the small error bars relative to the curve values. Hence, there were only minor variations in curve shape among the individual PIE curves sampled for each PAH. Accuracies cannot be defined since the total signal levels are arbitrary values that need to be calibrated to a reference. Therefore, the PIE curves have been normalized. The energy distribution of the ionizing photons, including the broad plateau of lower photon flux, yields a gradual ionization onset instead of a well-defined threshold. Hence,

sharp ionization thresholds cannot be established from the present measurements for any of the studied PAHs.

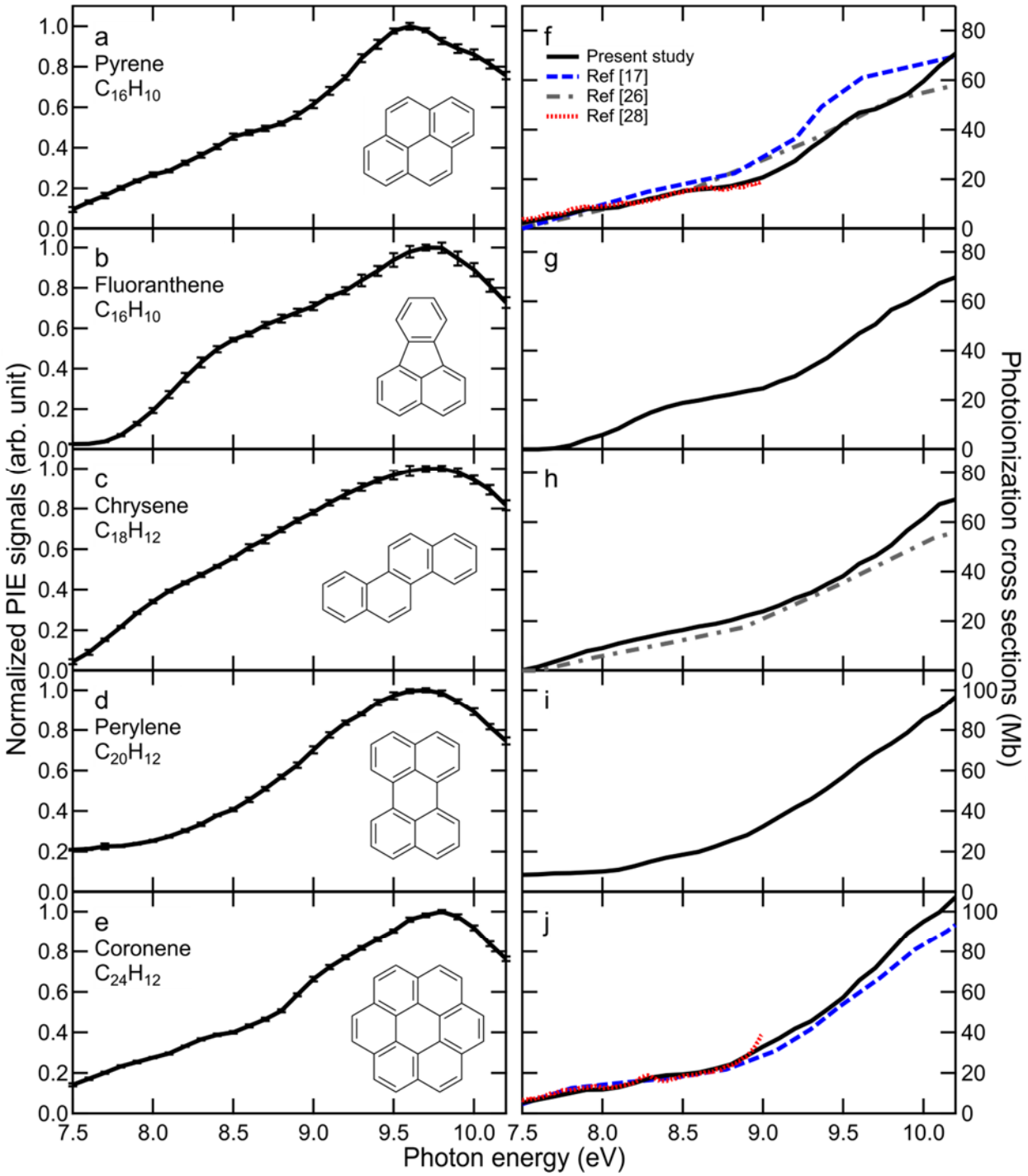

Fig. 3. Normalized measured PIE curves and inferred photoionization cross sections. (a-e) Averaged and normalized PIE curves are shown for each PAH species before photon-flux and background correction. The error bars show 95% confidence intervals of the standard errors of the mean of (a) 13 measurements for pyrene, (b) 12 for fluoranthene, (c) 8 for chrysene, (d) 11 for perylene, and (e) 19 for coronene. (f-j) Photoionization cross sections derived from the measurements shown in (a-e) are compared with measurements and estimations taken from the literature for (a) pyrene, (b) fluoranthene, (c) chrysene, (d) perylene, and (e) coronene. The solid black lines are derived from our measurements, and the broken lines are from Verstraete *et al*.[17] (blue dashed line), Li[26] (gray dot-dashed line), and Tobita *et al*.[28] (red dotted line) (see legend). See text for details.

Derivation of Photoionization Cross Sections

The PIE measurements shown in Figs. 3a-e do not provide information about the absolute photoionization cross sections, which requires knowledge of the abundance of the species of interest relative to a calibration substance in the ionization region.[34] In the present study, the concentration ratios between the 2,5-dimethylfuran and the PAH species are unknown. Aromatic species[17, 21-22, 35-39] and sub-micrometer sized graphite grains,[40] however, have a strong and broad absorption band that peaks near 17 eV. This absorption band has been attributed predominantly to $\sigma^* \leftarrow \sigma$ transitions and, to a lesser extent, to $\sigma^* \leftarrow \pi$ and $\pi^* \leftarrow \sigma$ transitions.[21-22, 37] The photoionization-quantum yield is virtually unity for all aromatic molecules near 17 eV.[17, 23] Malloci *et al*.[21] concluded that excitation to super-excited states that are coupled to the ionization continuum account for the majority of the absorption cross section of this band. At the peak of the

band, the absorption cross section per carbon atom is ~25 Mb,[21-22, 35-36] and the absorption cross section is, more or less, equal to the photoionization cross section because the photoionization yield is close to unity.[17, 23] The absorption cross-section calculations by Malloci *et al*.[21] include the five PAHs discussed here, and they all follow the trend of having absorption cross sections of approximately 25 Mb per carbon atom near 17 eV. Some PAHs, *e.g.*, coronene, have relatively sharp resonance features that yield somewhat higher maximum absorption cross section per carbon atom.[17, 21] Other PAHs may have relatively flat features near the top of their absorption curves and slightly lower peak absorption cross sections per carbon atom.[21] The exact value of the maximum absorption cross section per carbon atom, and the photon energy at which it occurs, vary somewhat among different PAHs. Nevertheless, the absorption cross section can be approximately set to a value near 25 Mb per carbon atom in the vicinity of 17 eV.

The MgF_2 window used in the present study prevented measurements to 17 eV. As an approximation, however, we assumed that the ratio between the photoionization cross sections at ~10 and 17 eV can be obtained from a linear increase between these two energies with slope and offset determined by the data points between ~9.8 and 10.2 eV. The true photoionization cross-section curves are expected to have features that yield local minima and maxima, but overall both the photoionization yield[17, 23] and the absorption cross section[21-22] increase between 10 and 17 eV. Thus, PAH photoionization cross-section curves steadily increase between 10 and 17 eV, albeit with some local minima and maxima, as shown by Verstraete *et al*.[17] for pyrene and coronene. The true shape of the photoionization cross-section curve with all of its local features is irrelevant for the present analysis, however, as long as the estimated slope and offset yield a ratio between the signal at ~10 eV and the extrapolated value at 17 eV that is close to the ratio between the true photoionization cross sections at these two energies.

The approach of extrapolating a straight line fit between 9.8 and 10.2 eV to 17 eV introduces uncertainty into our curve scaling. In order to test this approach, we used the absorption cross-section curves for pyrene, fluoranthene, chrysene, tetracene ($C_{18}H_{12}$), perylene, benzo[g,h,i]perylene ($C_{22}H_{12}$), anthanthrene ($C_{22}H_{12}$), pentacene ($C_{22}H_{14}$), and coronene taken from Malloci *et al.*[21] and the photoionization quantum-yield curve for coronene taken from Verstraete *et al*.[17] to estimate an average photoionization cross section per carbon atom. We selected these PAHs because they contain between 16 and 24 carbon atoms, *i.e.*, the size range spanned by the five PAHs under study. We divided each absorption cross-section curve by the number of carbon atoms in the corresponding structure and calculated the average of the curves in the photon-energy range 7.5 to 18 eV. The result is shown in Fig. 4 (dashed line), and the absorption cross section peaks at ~17 eV where the averaged curve has a value of ~23.9 Mb. The shaded area around the dashed line shows the standard deviation among the individual absorption cross-section curves per carbon atom. The averaged curve was then multiplied by the coronene photoionization quantum-yield curve from Verstraete *et al*.,[17] and the result is plotted in Fig. 4 (solid line). A linear extrapolation (dotted curve in Fig. 4) with slope and offset determined by the average photoionization curve between 9.8 and 10.2 eV yields an extrapolated value at 17 eV that is within 10% of the average photoionization curve value at this energy. This result supports our assumption that a linear extrapolation between ~10 and 17 eV should yield a representative ratio between the photoionization cross sections at these two photon energies for a PAH containing 16-24 carbon atoms.

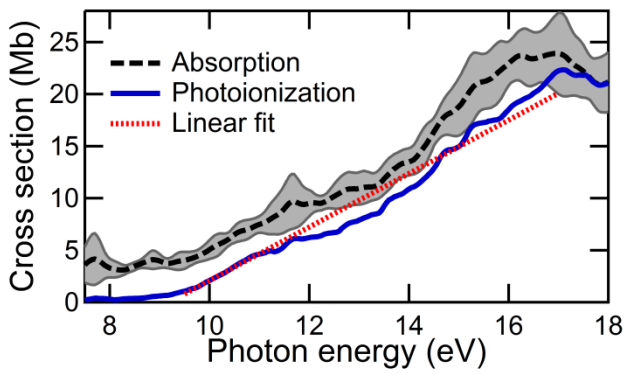

Fig. 4. Average absorption and photoionization cross-section curves per carbon atom. The average absorption cross section per carbon atom (dashed curve) was calculated using nine PAHs taken from Malloci *et al*.,[21] and the standard deviation among the individual curves is shown by the shaded gray area. The average photoionization curve (solid line) was obtained by multiplying the average absorption curve by the photoionization yield for coronene measured by Verstraete *et al.*[17] A linear extrapolation of the average photoionization curve from ~10 to 17 eV with slope and offset determined by a linear fit in the photon energy range of 9.8-10.2 eV is also shown (dotted curve). See text for details.

Prior to deriving slopes and offsets for the linear extrapolations, the measured PIE curves were corrected for differences in the photon flux at different photon energies. After photon-flux correction and extrapolation, the background of each averaged PAH-PIE curve was estimated, based on the knowledge that the photoionization cross section per carbon atom is nearly identical for the five species at 17 eV. Fluoranthene has an ionization energy (IE) of 7.9 eV,[41] and its photoionization cross section is therefore zero at 7.5 eV. Thus, each curve's background was estimated using the following equation:

$$bkg = \frac{N_{PAH}}{N_F}\frac{F(7.5)}{F(17)}PAH(17) \qquad (1)$$

In Eq. (1) N_F is the number of carbon atoms in fluoranthene, *i.e.*, 16, N_{PAH} is the number of carbon atoms in the species for which the background is calculated, $F(7.5)$ and $F(17)$ are the measured signal at 7.5 and the extrapolated value at 17 eV for fluoranthene (both taken prior to background subtraction, but after photon-flux correction), and $PAH(17)$ is the extrapolated value at 17 eV after photon-flux correction for the species for which the background is calculated. After subtracting the backgrounds, the PAH-PIE curves were set equal to $23.9N_C$ Mb at 17 eV, where N_C is the number of carbon atoms in their structures. The resulting photoionization cross-section curves are shown in Figs. 3f-j.

Figure 3 also shows photoionization cross-section curves reproduced from the literature for pyrene (Fig. 3f), chrysene (Fig. 3h), and coronene (Fig. 3j). The pyrene curves reproduced from the literature include an absolute measurement performed by Verstraete *et al.*,[17] a relative measurement reported by Tobita *et al.*,[28] and an estimation by Li.[26] Figure 3h compares an estimation for chrysene by Li[26] with our chrysene curve. We compare our coronene curve with an absolute measurement by Verstraete *et al.*[17] and a relative measurement performed by Tobita *et al.*[28] We obtained the curves reproduced from Verstraete *et al.*[17] and Li[26] from the Photoionization Cross Section Database webpage published by the Center for Advanced Combustion & Energy at the National Synchrotron Radiation Laboratory in Hefei, China (CACE)[42]. We interpolated the relative pyrene and coronene curves presented by Tobita *et al.*[28] using the original source. The measurements by Tobita *et al.*[28] include data points at photon energies below the ionization thresholds of pyrene and coronene, which eliminates ambiguity about their background and reduces the comparison between our measurements and theirs to a relative scaling factor. The

overall agreement between the present cross-section values for pyrene and coronene with earlier measurements indicate that our extrapolations of the photon-flux corrected PIE curves from ~10 eV to 17 eV yield reliable results for these two species. In addition, the presently derived chrysene photoionization cross sections are in relatively good agreement with the values of Li's[26] estimated curve.

The photoionization cross-section curve shapes derived for fluoranthene and perylene are as reliable as those derived for pyrene, chrysene, and coronene; the extrapolation to 17 eV does not influence the curve shapes. We expect the derived photoionization cross-section values to be in close agreement with the true values for all five species. Perylene (Fig. 3i) has the highest photoionization cross section near 7.5 eV of all of the five curves presented in Fig. 3f-j. This result is consistent with the low ionization threshold of perylene (6.96 eV)[43] compared to the four other PAH species; pyrene: 7.43 eV,[44] fluoranthene: 7.9 eV,[41] chrysene: 7.60 eV,[45] and coronene: 7.29 eV.[46]

Our pyrene measurements showed a dip in the photoionization cross-section curve between 8.5 and 9 eV. This dip is only weakly seen in the measurement by Verstraete *et al*.,[17] and it is not present in Li's[26] estimated curve. The curve reported by Verstraete *et al*.,[17] however, covers a very wide photon-energy range, and small local features are not resolved in the graph they published. Nevertheless, the relative pyrene measurement by Tobita *et al*.[28] contains a clear dip at the same photon energy as in our measurements and with nearly identical relative magnitude. These results indicate that this dip is present in the pyrene photoionization cross-section curve. In addition, the present measurement and the relative measurement by Tobita *et al*.[28] suggest that the pyrene photoionization cross section is slightly larger between 7.5 and 8 eV, relative to the values at higher photon energies, than indicated by the photoionization cross-section curves by Verstraete *et al*.[17]

and Li[26]. Above ~8.5 eV, our pyrene photoionization cross-section curve and those obtained by Verstraete *et al*.[17] and Li[26] display discrepancies in curve shapes. Furthermore, above ~9.6 eV, our pyrene curve has a steeper slope than the curves by Verstraete *et al*.[17] and Li[26]. In our experiments, the photon flux dropped off markedly at high photon energies, as seen in Fig. 1 and Fig. 3a-e, which makes the high-energy region susceptible to errors in the photon-flux correction. Nevertheless, as argued below, it seems unlikely that errors in the photon-flux correction alone could explain the observed differences between the currently derived curve and the pyrene curve presented by Verstraete *et al*.,[17] which also disagrees with Li's[26] estimated curve at the higher-photon energies. Li's[26] curve does not reproduce the steeper increase in photoionization cross-section seen between ~9 and 9.5 eV for both our data and the curve presented by Verstraete *et al*.[17]

Our derived chrysene photoionization cross-section curve in Fig. 3h is consistently higher than Li's[26] estimation for this species. Hence, as a further test of our results, we used the atom-pair additivity model of Bobeldijk *et al*.[24] to estimate the photoionization cross section without relying on the extrapolation of our curves to 17 eV. This approach requires a reference photoionization cross-section value for each atom pair. The total photoionization cross section at the reference photon energy is then calculated by summing the contributions from all of the atom pairs in the molecule. After photon-flux and background correction, a measured PIE curve can be scaled so that it matches the calculated photoionization cross section at the reference photon energy. Benzene is the simplest aromatic species, and its photoionization cross section has been reported in the literature, see, *e.g.*, Cool *et al.*[34] and Rennie *et al.*[47] Thus, as a starting point, benzene may serve as the reference species for the atom-pair additivity model. The ionization threshold of benzene is ~9.2 eV, as measured by Cool *et al.*[34] and Rennie *et al.*[47] There are some discrepancies between these two studies. Therefore, we use the average of the two curves, which yields ~12.1

Mb at 9.5 eV. The photoionization cross section is assumed to be equally distributed over the 6 carbon-carbon atom pairs, because the contributions from the carbon-hydrogen atom pairs are assumed to be zero at the photon energies used in the present study (7.5-10.2 eV).[24] Hence, using benzene at 9.5 eV as the reference, the atom-pair additivity model predicts a photoionization cross section of ~42.5 Mb at 9.5 eV for chrysene, whereas the value derived from our data is 38.2 Mb, and the interpolated value from Li's[26] estimated curve is 35.6 Mb. Using the benzene photoionization cross section at 10 eV (~23.8 Mb, average between the photoionization cross sections reported by Cool *et al*.[34] and Rennie *et al*.[47]) as the reference yields a photoionization cross section of ~83.5 Mb, which is about 22 Mb higher than our derived photoionization cross section at 10 eV and ~32 Mb higher than the corresponding value from Li.[26]

Using the benzene photoionization cross-section curve as a reference for the atom-pair additivity model yields a rescaled curve that has the exact same shape as the original benzene photoionization cross-section curve. This rescaled benzene curve may be in agreement with chrysene's photoionization cross section at some photon energies, but is unlikely to be representative of the chrysene photoionization cross-section curve over any significant energy range near 9 eV because of benzene's high ionization threshold. Alternatively, we can use the average between our pyrene curve and the pyrene curve from Verstraete *et al*.[17] as the reference for chrysene. Figure 3 shows that the photoionization cross-section curve shapes of pyrene and chrysene are similar although the pyrene curve contains more pronounced local features. Because the two pyrene curves are in closer agreement at low photon energies than at high photon energies (Fig. 3f), we use 8.5 eV as the reference energy. The average pyrene photoionization cross section at this energy is 16.6 Mb, which yields a chrysene photoionization cross section of 18.3 Mb if all the carbon-carbon bonds contribute equally. This value is only slightly higher than the 16.4 Mb presently obtained for

chrysene at 8.5 eV (Fig. 3h), but almost 50% higher than the 12.4 Mb predicted by Li.[26] Not treating all the carbon-carbon bonds equally would likely have resulted in a different scaling factor between chrysene and pyrene that could potentially have brought the value obtained from the atom-pair additivity model closer to Li's[26] prediction. Nevertheless, not treating the carbon-carbon bonds equally would have required information on the relative photoionization cross sections between carbon-carbon bonds of different bond lengths in aromatic species.

The selection of pyrene as a reference is an arbitrary choice. If the average coronene photoionization cross section at 8.5 eV (18.8 Mb) is used, the atom-pair additivity model predicts a chrysene photoionization cross section of 13.2 Mb, which is in closer agreement with Li's[26] estimation (12.4 Mb) than with our derived value at this photon energy (16.4 Mb). Our coronene cross section and that reported by Verstraete *et al*.[17] are in close agreement also at 9.5 eV, and the average between the two curves is 55.6 Mb at this energy. Hence, using the average coronene photoionization cross section at 9.5 eV yields a predicted chrysene photoionization cross section of 38.9 Mb, which is in agreement with our chrysene cross section value of 38.2 Mb. At 9.5 eV, Li's[26] estimation is ~35.6 Mb.

The inconsistencies in the estimations using the atom-pair additivity model illustrate one of the shortcomings of estimating photoionization cross sections. The photoionization cross-section curves in Fig. 3 show that different PAHs have slightly different photoionization cross-section curve shapes. The atom-pair additivity model, as it has presently been applied, will thus perform differently for different PAHs, and the differences in performance will depend on the photon energy. Additional work may be required to verify our chrysene cross section values and allow rescaling to account for any mismatch.

The derived coronene photoionization cross-section curve is in agreement with the measurement by Verstraete *et al*.[17] between 7.5 and ~9.5 eV and with the curve measured by Tobita *et al*.[28] between 7.5 and ~8.9 eV. Tobita *et al*.[28] only measured to 9 eV, but their curve increases sharply at ~8.9 eV and diverges from the other two measurements in Fig. 3j. Beyond ~9.5 eV, our coronene curve is somewhat higher than the curve by Verstraete *et al*.[17] As in the case of pyrene, our coronene curve increases slightly faster with increasing photon energy above ~9.5 eV than the curve by Verstraete *et al*.[17] The difference in rate of increase between our curves and the curves by Verstraete *et al*.[17] is smaller for coronene than for pyrene, suggesting that it is unlikely that the discrepancies between our measurements and those measured by Verstraete *et al*.[17] beyond ~9.5 eV for pyrene and coronene are due only to errors in our photon-flux references. It seems more likely that the limited resolution of the pyrene and coronene curves provided in the original source by Verstraete et al.[17] has larger impact on local curve features than any errors in our photon-flux corrections.

SUMMARY AND CONCLUSIONS

We have inferred photoionization cross-section curves for pyrene, fluoranthene, chrysene, perylene, and coronene in the photon energy range 7.5-10.2 eV from measurements of PIE curves for these species. Photon-flux references were obtained from concurrent PIE measurements on 2,5-dimethylfuran. In order to obtain quantitative values, the photon-flux corrected curves were extrapolated from ~10 to 17 eV where the photoionization cross section per carbon atom was set to 23.9 Mb after background subtraction. Our results demonstrate good agreement with earlier measurements and estimations of the photoionization cross-section curves of pyrene and

coronene,[17,28] providing support for the applicability of our approach for derivation of PAH photoionization cross sections.

ACKNOWLEDGMENT

This work was funded by the U.S. Department of Energy (DOE), Office of Basic Energy Sciences (BES). KOJ, PE, and AV were supported by the Single Investigator Small Group Research (SISGR), Grant no. DE-SC0002619. MFC, PES, JZ, HAM, and experimental expenses were funded under DOE BES, the Division of Chemical Sciences, Geosciences, and Biosciences. The ALS, NKRH, and KRW were supported by the Director, DOE BES, under Contract no. DE-AC02-05CH11231. Sandia National Laboratories is a multi-mission laboratory managed and operated by National Technology and Engineering Solutions of Sandia, LLC., a wholly owned subsidiary of Honeywell International, Inc., for the U.S. Department of Energy's National Nuclear Security Administration under contract DE-NA0003525.

REFERENCES

(1) Seinfeld, J. H.; Pandis, S. N. *Atmospheric Chemistry and Physics: From Air Pollution to Climate Change*. John Wiley & Sons: New York, **1998**.
(2) Finlayson-Pitts, B. J.; Pitts, J. N., Jr *Chemistry of the Upper and Lower Atmosphere: Theory, Experiment, and Applications*. Academic Press: San Diego, **2000**.
(3) Finlayson-Pitts, B. J.; Pitts, J. N. Tropospheric Air Pollution: Ozone, Airborne Toxics, Polycyclic Aromatic Hydrocarbons, and Particles. *Science* **1997,** *276*, 1045-1051.
(4) Richter, H.; Howard, J. B. Formation of Polycyclic Aromatic Hydrocarbons and Their Growth to Soot—a Review of Chemical Reaction Pathways. *Prog. Energy Combust. Sci.* **2000,** *26*, 565-608.
(5) Michelsen, H. Probing Soot Formation, Chemical and Physical Evolution, and Oxidation: A Review of *in Situ* Diagnostic Techniques and Needs. *Proc. Combust. Inst.* **2017,** *36*, 717-735.
(6) Wang, H. Formation of Nascent Soot and Other Condensed-Phase Materials in Flames. *Proc. Combust. Inst.* **2011,** *33*, 41-67.
(7) D'Anna, A. Combustion-Formed Nanoparticles. *Proc. Combust. Inst.* **2009,** *32*, 593-613.

(8) Léger, A.; Puget, J. Identification of the 'Unidentified' IR Emission Features of Interstellar Dust? *Astron. Astrophys.* **1984,** *137*, L5-L8.
(9) Allamandola, L.; Tielens, A.; Barker, J. Polycyclic Aromatic Hydrocarbons and the Unidentified Infrared Emission Bands-Auto Exhaust Along the Milky Way. *Astrophys. J.* **1985,** *290*, L25-L28.
(10) Tielens, A. G. Interstellar Polycyclic Aromatic Hydrocarbon Molecules. *Annu. Rev. Astron. Astrophys.* **2008,** *46*, 289-337.
(11) Ehrenfreund, P.; Charnley, S. B. Organic Molecules in the Interstellar Medium, Comets, and Meteorites: A Voyage from Dark Clouds to the Early Earth. *Annu. Rev. Astron. Astrophys.* **2000,** *38*, 427-483.
(12) Allamandola, L.; Hudgins, D.; Sandford, S. Modeling the Unidentified Infrared Emission with Combinations of Polycyclic Aromatic Hydrocarbons. *The Astrophysical Journal Letters* **1999,** *511*, L115.
(13) Puget, J.; Léger, A. A New Component of the Interstellar Matter-Small Grains and Large Aromatic Molecules. *Annu. Rev. Astron. Astrophys.* **1989,** *27*, 161-198.
(14) Allamandola, L.; Tielens, A.; Barker, J. Interstellar Polycyclic Aromatic Hydrocarbons-the Infrared Emission Bands, the Excitation/Emission Mechanism, and the Astrophysical Implications. *Astrophys. J. Suppl. Ser.* **1989,** *71*, 733-775.
(15) d'Hendecourt, L.; Léger, A. Effect of Photoionization of PAH Molecules on the Heating of HI Interstellar Gas. *Astron. Astrophys.* **1987,** *180*, L9-L12.
(16) Bakes, E.; Tielens, A. The Photoelectric Heating Mechanism for Very Small Graphitic Grains and Polycyclic Aromatic Hydrocarbons. *Astrophys. J.* **1994,** *427*, 822-838.
(17) Verstraete, L.; Léger, A.; d'Hendecourt, L.; Defourneau, D.; Dutuit, O. Ionization Cross-Section Measurements for Two PAH Molecules-Implications for the Heating of Diffuse Interstellar Gas. *Astron. Astrophys.* **1990,** *237*, 436-444.
(18) Mebel, A. M.; Landera, A.; Kaiser, R. I. Formation Mechanisms of Naphthalene and Indene: From the Interstellar Medium to Combustion Flames. *J. Phys. Chem. A* **2017**.
(19) Zhang, F.; Kaiser, R. I.; Kislov, V. V.; Mebel, A. M.; Golan, A.; Ahmed, M. A VUV Photoionization Study of the Formation of the Indene Molecule and Its Isomers. *J. Phys. Chem. Lett.* **2011,** *2*, 1731-1735.
(20) Parker, D. S.; Kaiser, R. I.; Troy, T. P.; Ahmed, M. Hydrogen Abstraction/Acetylene Addition Revealed. *Angew. Chem. Int. Ed.* **2014,** *53*, 7740-7744.
(21) Malloci, G.; Mulas, G.; Joblin, C. Electronic Absorption Spectra of PAHs up to Vacuum UV-Towards a Detailed Model of Interstellar PAH Photophysics. *Astron. Astrophys.* **2004,** *426*, 105-117.
(22) Malloci, G.; Joblin, C.; Mulas, G. Theoretical Evaluation of PAH Dication Properties. *Astron. Astrophys.* **2007,** *462*, 627-635.
(23) Jochims, H.; Baumgärtel, H.; Leach, S. Photoionization Quantum Yields of Polycyclic Aromatic Hydrocarbons. *Astron. Astrophys.* **1996,** *314*, 1003-1009.
(24) Bobeldijk, M.; Van der Zande, W.; Kistemaker, P. Simple Models for the Calculation of Photoionization and Electron Impact Ionization Cross Sections of Polyatomic Molecules. *Chem. Phys.* **1994,** *179*, 125-130.
(25) Johansson, K. O.; Dillstrom, T.; Elvati, P.; Campbell, M. F.; Schrader, P. E.; Popolan-Vaida, D. M.; Richards-Henderson, N. K.; Wilson, K. R.; Violi, A.; Michelsen, H. A. Radical-Radical Reactions, Pyrene Nucleation, and Incipient Soot Formation in Combustion. *Proc. Combust. Inst.* **2017,** *36*, 799-806.

(26) Li, Y. Estimated Photoionization Cross Sections, Photonionization Cross Section Database (Version 1.0). Center for Advanced Combustion & Energy (CACE): National Synchrotron Radiation Laboratory, Hefei, China, **2011**. http://flame.nsrl.ustc.edu.cn/database/ (accessed May 2016).
(27) Johansson, K. O.; Lai, J. Y. W.; Skeen, S. A.; Popolan-Vaida, D. M.; Wilson, K. R.; Hansen, N.; Violi, A.; Michelsen, H. A. Soot Precursor Formation and Limitations of the Stabilomer Grid. *Proc. Combust. Inst.* **2015,** *35*, 1819-1826.
(28) Tobita, S.; Leach, S.; Jochims, H.; Rühl, E.; Illenberger, E.; Baumgärtel, H. Single-and Double-Ionization Potentials of Polycyclic Aromatic Hydrocarbons and Fullerenes by Photon and Electron Impact. *Can. J. Phys.* **1994,** *72*, 1060-1069.
(29) Headrick, J. M.; Schrader, P. E.; Michelsen, H. A. Radial-Profile and Divergence Measurements of Combustion-Generated Soot Focused by an Aerodynamic-Lens System. *J. Aerosol Sci.* **2013,** *58*, 158-170.
(30) Zhang, X.; Smith, K. A.; Worsnop, D. R.; Jimenez, J. L.; Jayne, J. T.; Kolb, C. E.; Morris, J.; Davidovits, P. Numerical Characterization of Particle Beam Collimation: Part II Integrated Aerodynamic-Lens–Nozzle System. *Aerosol Sci. Technol.* **2004,** *38*, 619-638.
(31) Liu, P. S.; Deng, R.; Smith, K. A.; Williams, L. R.; Jayne, J. T.; Canagaratna, M. R.; Moore, K.; Onasch, T. B.; Worsnop, D. R.; Deshler, T. Transmission Efficiency of an Aerodynamic Focusing Lens System: Comparison of Model Calculations and Laboratory Measurements for the Aerodyne Aerosol Mass Spectrometer. *Aerosol Sci. Technol.* **2007,** *41*, 721-733.
(32) Xie, M.; Zhou, Z.; Wang, Z.; Chen, D.; Qi, F. Determination of Absolute Photoionization Cross-Sections of Oxygenated Hydrocarbons. *Int. J. Mass spectrom.* **2010,** *293*, 28-33.
(33) Audi, G.; Wapstra, A. The 1995 Update to the Atomic Mass Evaluation. *Nucl. Phys. A* **1995,** *595*, 409-480.
(34) Cool, T. A.; Wang, J.; Nakajima, K.; Taatjes, C. A.; Mcllroy, A. Photoionization Cross Sections for Reaction Intermediates in Hydrocarbon Combustion. *Int. J. Mass spectrom.* **2005,** *247*, 18-27.
(35) Cecchi-Pestellini, C.; Malloci, G.; Mulas, G.; Joblin, C.; Williams, D. The Role of the Charge State of PAHs in Ultraviolet Extinction. *Astron. Astrophys.* **2008,** *486*, L25-L29.
(36) Koch, E.-E.; Otto, A. Vacuum Ultra-Violet and Electron Energy Loss Spectroscopy of Gaseous and Solid Organic Compounds. *Int. J. Radiat. Phys. Chem.* **1976,** *8*, 113-150.
(37) Verstraete, L.; Léger, A. The Visible and Ultraviolet Absorption of Large Polycyclic Aromatic Hydrocarbons. *Astron. Astrophys.* **1992,** *266*, 513-519.
(38) Koch, E.-E.; Otto, A.; Radler, K. The Vacuum Ultraviolet Spectrum of Naphthalene Vapour for Photon Energies from 5 to 30 eV. *Chem. Phys. Lett.* **1972,** *16*, 131-135.
(39) Yoshino, M.; Takeuchi, J.; Suzuki, H. Absorption Cross Sections and Photoionization Efficiencies of Benzene and Styrene Vapor in the Vacuum Ultraviolet. *J. Phys. Soc. Jpn.* **1973,** *34*, 1039-1044.
(40) Draine, B.; Lee, H. M. Optical Properties of Interstellar Graphite and Silicate Grains. *Astrophys. J.* **1984,** *285*, 89-108.
(41) Ling, Y.; Lifshitz, C. Time-Dependent Mass Spectra and Breakdown Graphs. 19. Fluoranthene. *J. Phys. Chem.* **1995,** *99*, 11074-11080.
(42) Photonionization Cross Section Database (Version 1.0). Center for Advanced Combustion & Energy (CACA): National Synchrotron Radiation Laboratory, Hefei, China, **2011**. http://flame.nsrl.ustc.edu.cn/database/ (accessed May 2016).

(43) Shchuka, M. I.; Motyka, A. L.; Topp, M. R. Two-Photon Threshold Ionization Spectroscopy of Perylene and Van Der Waals Complexes. *Chem. Phys. Lett.* **1989,** *164*, 87-95.
(44) Hager, J. W.; Wallace, S. C. Two-Laser Photoionization Supersonic Jet Mass Spectrometry of Aromatic Molecules. *Anal. Chem.* **1988,** *60*, 5-10.
(45) Shahbaz, M.; Akiyama, I.; LeBreton, P. Ultraviolet Photoelectron Studies of Methyl Substituted Crysenes. *Biochem. Biophys. Res. Commun.* **1981,** *103*, 25-30.
(46) Clar, E.; Robertson, J.; Schlögl, R.; Schmidt, W. Photoelectron Spectra of Polynuclear Aromatics. 6. Applications to Structural Elucidation:" Circumanthracene". *J. Am. Chem. Soc.* **1981,** *103*, 1320-1328.
(47) Rennie, E.; Johnson, C.; Parker, J.; Holland, D.; Shaw, D.; Hayes, M. A Photoabsorption, Photodissociation and Photoelectron Spectroscopy Study of C_6H_6 and C_6D_6. *Chem. Phys.* **1998,** *229*, 107-123.

TOC Graphic